frontiers | Frontiers in Materials

TYPE Original Research
PUBLISHED 22 September 2025
DOI 10.3389/fmats.2025.1684508

OPEN ACCESS

EDITED BY
Jue Li,
Chongqing Jiaotong University, China

REVIEWED BY
Naitian Zhang,
Xinjiang University, China
Huijie Lv,
Ningxia University, China
Xiyan Fan,
Changsha University of Science and Technology, China

*CORRESPONDENCE
Pengfei Li,
2089250145@qq.com

RECEIVED 12 August 2025
ACCEPTED 08 September 2025
PUBLISHED 22 September 2025

CITATION
Jin W, Song S, Li P, Shan J and Xing C (2025) Study on mechanical properties and luminescence function of pouring energy-storage luminescent asphalt mixture. *Front. Mater.* 12:1684508.
doi: 10.3389/fmats.2025.1684508

Study on mechanical properties and luminescence function of pouring energy-storage luminescent asphalt mixture

Wenliang Jin[1], Shenyou Song[2], Pengfei Li[3,4]*, Jinhuan Shan[3,4] and Chengwei Xing[3,4]

[1]Shenzhen-Zhongshan Link Administration Center, Zhongshan, China, [2]Guangdong Highway Construction Co., Ltd, Guangzhou, China, [3]Key Laboratory for Special Area Highway Engineering of Ministry of Education, Chang'an University, Xi'an, China, [4]School of Highway, Chang'an University, Xi'an, China

Energy-storage luminescent pavements can provide illumination in dark or low-light environments, aiding drivers and pedestrians in better recognizing road conditions and thereby reducing the occurrence of traffic accidents. The pouring energy-storage luminescent asphalt mixture (PELAM) proposed in this study comprises a porous asphalt mixture matrix and long-afterglow-epoxy resin grouting material filling the voids within it. The mechanical properties of the mixture were studied through dynamic modulus, phase angle, and repeated loading creep tests; the effects of different void ratios, immersion times, and weather conditions on the afterglow brightness of the specimens were tested to analyze the impact on luminescent function. The results show that the dynamic modulus of PELAM gradually increases with the decrease of the test temperature, the increase of the loading frequency and the increase of the void ratio. The Phase angle changes lack a clear pattern with temperature and frequency variations. The flow number and the micro-strain corresponding to the flow number gradually increase with the increase of the void ratio. The void ratio and short-term immersion have little influence on the afterglow effect of pouring energy-storage luminescent asphalt mixture, and 21 days of immersion slightly reduces the afterglow brightness; under the excitation of natural light, the afterglow duration can last for more than 6 hours. The mechanical properties and luminescent function of PELAM are suitable for pavement applications.

KEYWORDS

road engineering, pouring energy-storage luminescent asphalt mixture, mechanical properties, luminescent performance, afterglow brightness

1 Introduction

The safety of night driving has always been an important issue. Due to insufficient night lighting, it is difficult for drivers to see the road conditions, which can lead to traffic accidents. Developing materials and technologies that enhance the visibility of roads at night will provide great convenience for pedestrians and unlit vehicles at night (Li et al., 2024). The luminescent characteristics of self-luminous pavement materials play an important role in auxiliary lighting and improving road safety.

The self-luminous material absorbs a certain wavelength of light and enters an excited state, and then emits visible light (Jiang et al., 2023a). According to the different application scenarios, the road surface is mainly divided into self-luminous coating (Ling et al., 2022), embedded self-luminous gravel (Chen et al., 2023), cement-based self-luminous material (Wang et al., 2023a) and epoxy resin-based self-luminous material (Jiang et al., 2023b). Among them, the construction of self-luminous coatings is relatively simple and can be applied to various road surfaces, but the wear resistance of the materials is insufficient, which adversely affects the duration of luminescence (Li et al., 2022); embedded self-luminous aggregates are pressed into the pavement during formation and can be pre-assembled into various patterns, presenting rich visual effects, but their laying difficulty is high and the application cost is high (Caputo et al., 2020); cement-based self-luminous materials have poor translucency under the action of cement coverage, affecting the brightness of luminescence (Wang et al., 2022b). Epoxy resin-based self-luminous materials combine epoxy resin with luminescent materials, with the advantages of good translucency, high luminance, and good flexibility and toughness, showing good application prospects.

The pouring energy-storage luminescent asphalt mixture (PELAM) is to pour the epoxy resin-based self-luminous material into the void structure of the porous asphalt mixture, which not only takes into account the road performance of the asphalt mixture but also has luminescent functions, reducing the wear of the self-luminous material and extending its service life. The pouring pavement structure has the advantages of good anti-rutting performance, oil and acid pollution resistance, water stability, low construction cost, and wide application range (Li et al., 2025). It not only improves the carrying capacity and service life of roads but also reduces maintenance costs, providing a strong guarantee for the safety and smooth flow of road traffic (Shan et al., 2024).

At present, research on pouring pavement structures is mainly focused on cement-based grout materials. Cai et al. (2017) proposed the optimal proportion component ratio for the cement grunt used in perfused asphalt pavements based on optimization principles. Zheng et al. (2023) developed a high-performance permeable pavement material for heavy-load scenarios, and the rut depth under the same conditions was only 1/10 of the SMA paving structure. Wang et al. (2023b) analyzed the adhesion interaction between the grouting material and the asphalt surface, thereby offering a theoretical foundation for exploring the cracking damage in permeable pavements. Ling et al. (2021) found that the interfacial cracks of cement-asphalt-aggregate are the main failure mode of the permeable asphalt mixture, and it is recommended that the void ratio of porous asphalt mixture be selected at about 25% when the permeable pavement is used for light traffic.

In addition, other types of grouting materials are also used in pavements, such as geopolymer grouting materials with high strength (Hamid et al., 2023), low shrinkage (Wang et al., 2022b), and impermeability (Sharkawi et al., 2020). This grouting material can not only effectively improve the bearing capacity and durability of the pavement but also significantly reduce the risk of cracks caused by material shrinkage, thereby extending the service life of the pavement (Zhang et al., 2021). Polyethylene terephthalate (PET) grouting materials have good weather resistance and chemical corrosion resistance (Khan et al., 2021). This material is not biodegradable and its use in pavement structures promotes the effective utilization of waste plastics (Mishra and Gupta, 2018). This measure not only helps reduce environmental pollution but also promotes the development of the circular economy and makes a positive contribution to environmental protection. Polyurethane grouting materials have strong permeability and can quickly penetrate pavement cracks and pores to form a tight bonding layer (Al-shawafi et al., 2023). At the same time, polyurethane grouting materials also have excellent bonding effects and waterproof performance and can maintain good bonding strength even on humid interfaces (Cavalli et al., 2023). These characteristics make polyurethane grouting materials play an important role in pavement crack repair (Li et al., 2020), board bottom void repair (Liu et al., 2023), and soft layer reinforcement (Saleh et al., 2019), effectively improving the overall performance and safety of the pavement (Xiong et al., 2024). Epoxy resin-based self-luminous grouting materials make the pavement realize the function of self-luminescence, but at present, there are relatively few application studies on pouring energy-storage luminescent asphalt mixture.

When functional materials are applied to pavement structures, their impact on the mechanical properties of the pavement and the performance of their functions are also important research directions (Dalhat and Al-Adham, 2023). For example, when self-healing capsules are applied to pavement repair, multi-chamber microcapsules with a size comparable to the gaps in asphalt mixtures have a small impact on the mechanical properties of asphalt mixtures and have a sustained release effect (He et al., 2020). Phase change materials regulate pavement temperature, and solid-liquid phase change materials produce a liquid phase that is easy to flow during phase transition, causing the asphalt to soften, which harms the performance of asphalt and its mixtures (Zhang et al., 2023); solid-solid phase change materials do not affect the structure of the pavement itself due to volume changes, so they are easier to apply to road engineering than solid-liquid phase change materials (Jia et al., 2023). Therefore, the influence of epoxy resin-based self-luminous grouting material injected into porous pavement structure on the mechanical properties of the asphalt mixture and the maintenance of the luminous function are the key to its application on the pavement.

In summary, a thorough analysis of both the mechanical and luminescent capabilities of self-luminous asphalt mixtures is necessary, this paper prepared PELAM and tested the mechanical properties and luminescent properties under different conditions using mechanical and optical test methods. The bearing capacity and deformation resistance of PELAM under different stress conditions were evaluated, and key performance indicators such as afterglow brightness and luminescent duration were measured. The research results provide ideas and references for the promotion and application of PELAM.

2 Materials and methods

2.1 Experimental materials

2.1.1 Epoxy resin based energy-storage luminescent grout

The epoxy resin based energy-storage luminescent grout material was mainly consists of epoxy resin, curing agent,

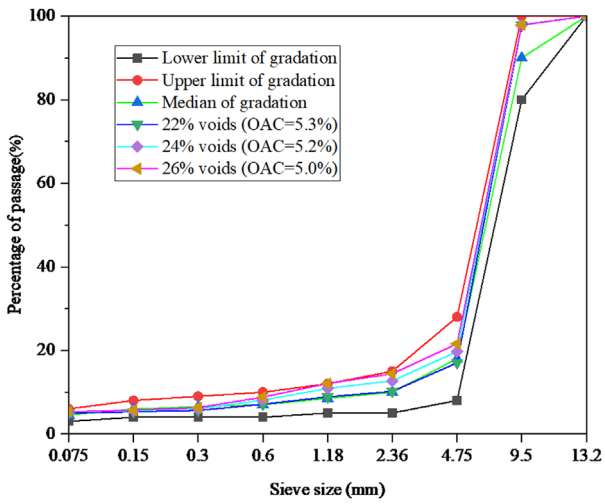

FIGURE 1
Gradation Curve of PAC-10.

toughening agent, and energy-storage long persistent luminescence material (LPL). To ensure that the grouting material has good translucency and mechanical properties, bisphenol A typed E51 epoxy resin, amine typed 593B curing agent, and DBP typed toughening agent were chosen as the binding agents; in order to make the grouting material have high afterglow luminosity and prolonged afterglow duration, $SrAl_2O_4$:Eu,Dy, an aluminate-based LPL, was selected as the additive. The components in the grout is as follows: E51: 593B: DBP:LPL = 100:18:15:14. At 25 °C, the epoxy resin and toughening agent were first mixed in proportion and stirred at 500 rpm for 10 min. Subsequently, the curing agent was added and stirred at 300 rpm for 5 min to form an adhesive system. Finally, long-afterglow material was incorporated into the mixture, which was stirred at 300 rpm for another 5 min to achieve uniform dispersion. After thorough mixing, vacuum defoaming was performed to obtain the epoxy resin-based self-luminescent grout.

2.1.2 Porous asphalt mixture

Porous asphalt mixture serves as the matrix, within which the voids provide ample space for the epoxy resin energy-storage luminescent grout. To maximize the utilization of the grouting material, this study selects PAC-10 porous asphalt mixture with a nominal maximum particle size of 10 mm, and controls the pouring thickness at 20 mm, ensuring that only the surface layer of the pavement material can emit light. To identify the optimal balance between economic efficiency and the energy-storage luminescent effect, three different target void ratios were designed, namely 22%, 24%, and 26%. The corresponding gradation curves are presented in Figure 1.

2.2 Preparation of pouring energy-storage luminescent asphalt mixture

Figure 2 illustrates the preparation process of PELAM. Firstly, In order to prevent the grouting material from flowing out through the interconnected voids at the bottom or sides of the specimen during the grouting process, waterproof adhesive tape was applied to the sides and bottom of the specimen. Subsequently, an appropriate amount of epoxy resin based energy-storage luminescent grout is evenly poured onto the surface of the specimen. The specimen was left to stand for 2 h to allow it to fully penetrate into the internal voids of the specimen under the action of gravity. When the grouting material at the top is no longer penetrating, the excess material on the surface of the specimen is gently scraped off to form the desired texture depth. Then, the specimen is left at 25 °C for 48 h to facilitate the complete curing of the epoxy resin, ultimately resulting in an asphalt mixture with energy-storage luminescent properties.

2.3 Mechanical property test

Take a core of the PELAM with a height of 150 mm and a diameter of 100 mm. Use a UTM-30 type dynamic servo-hydraulic tester to test the dynamic modulus and phase angle of the specimen, with test temperatures of 5 °C, 20 °C, and 35 °C, and loading frequencies of 0.1 Hz, 0.5 Hz, 1 Hz, 5 Hz, 10 Hz, and 25 Hz.

Use the same method as the dynamic modulus test to prepare the specimen, place the specimen in the UTM-30 tester at 55 °C for 6 h, and use a half-sine wave with an axial loading pressure value of 700 kPa to load the specimen with different void ratios, each cycle loads for 0.1 s, then unloads for 0.9 s, completes 5,000 cycles of the creep recovery process, and obtains the flow number and corresponding microstrain.

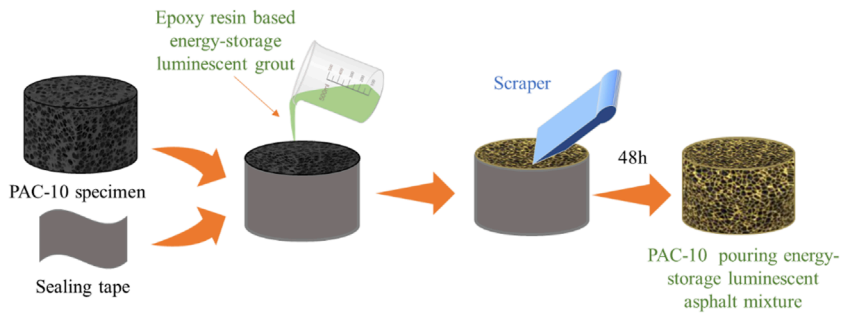

FIGURE 2
Preparation of pouring energy-storage luminescent asphalt mixture.

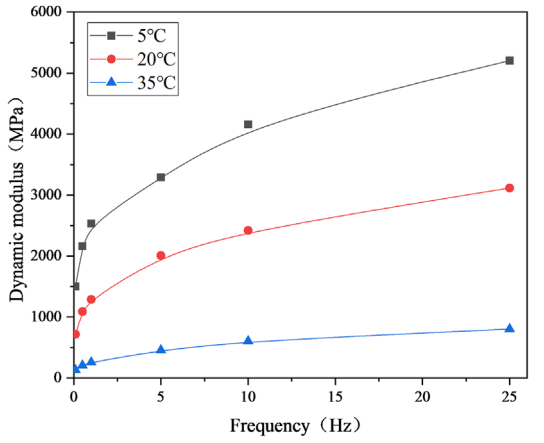

(a) 22%

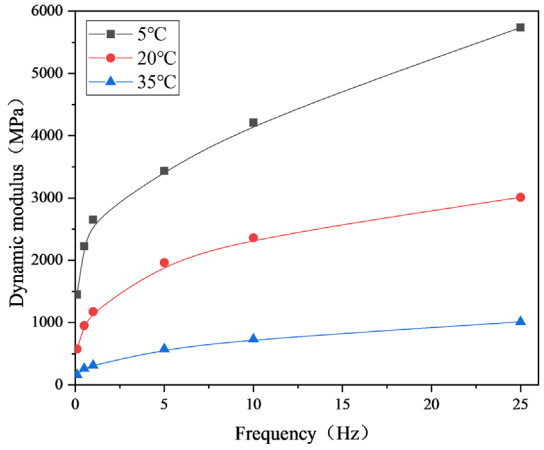

(b) 24%

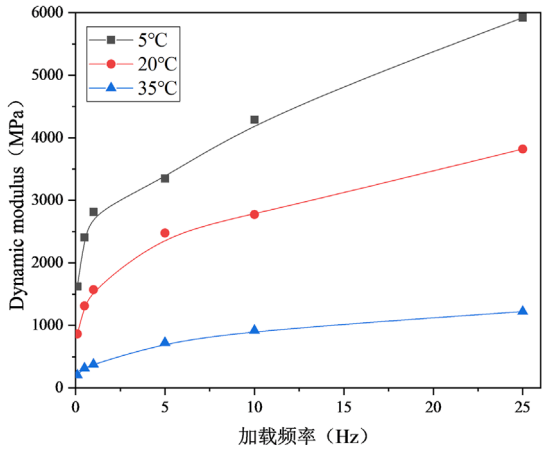

(c) 26%

FIGURE 3
Dynamic modulus of PELAM specimens with different void voids.

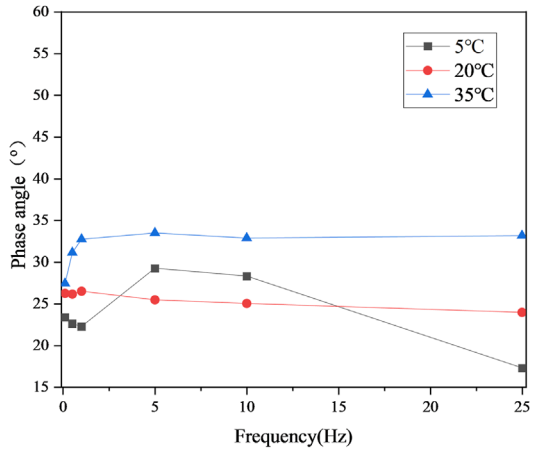

(a) 22%

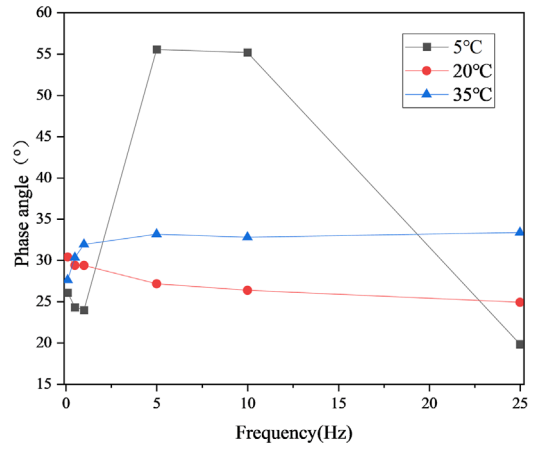

(b) 24%

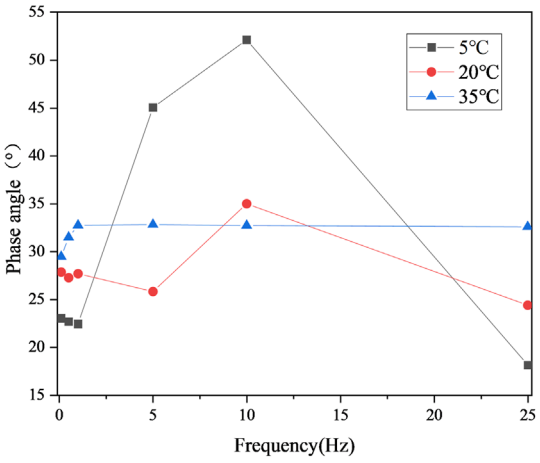

(c) 26%

FIGURE 4
Phase angle of PELAM specimens with different void ratios.

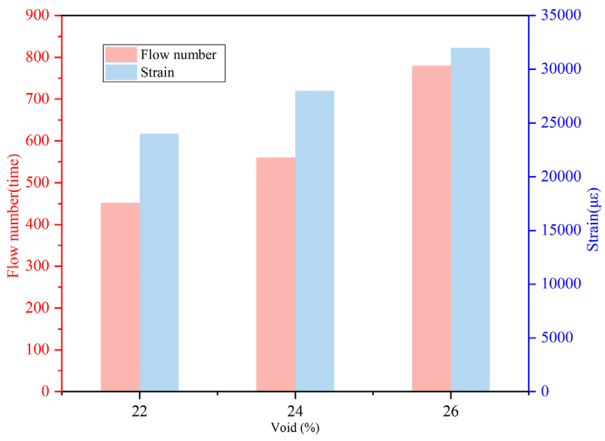

FIGURE 5
Repeated loading creep results of PELAM specimens with different void ratios.

2.4 Luminescent function test

To ensure that the long-afterglow material absorbs ultraviolet (UV) energy sufficiently for effective excitation and subsequent emission of optimal brightness, the specimens were placed in an ultraviolet chamber. The specimens' surfaces were exposed to ultraviolet radiation with a wavelength of 365 nm for a duration of 30 min, with the UV light source positioned at a distance of 10 cm from the top of the specimens. After the irradiation process, the light source was deactivated, and a brightness meter was employed to assess how the afterglow brightness of specimens with different void ratios decreased over time.

In addition, the specimens were immersed in water at 25 °C, with the surface of the specimens at a depth of 10 cm from the water surface. The immersion times were 7 days, 14 days and 21 days respectively. The attenuation of afterglow brightness of the specimens at different immersion times was tested.

Place the specimen in an outdoor space, and use a radiometer to test the change of solar radiation intensity within 1 day. After the absence of solar radiation, place the specimen in a dark environment, and test the afterglow brightness of the specimen over time.

3 Results and discussion

3.1 Mechanical property analysis

3.1.1 Dynamic modulus

The dynamic modulus of PELAM with void ratios of 22%, 24%, and 26%, under different temperatures and loading frequencies, was shown in Figure 3. Under the same loading frequency, the dynamic modulus of each specimen decreased gradually with the increase of test temperature. The epoxy resin self-luminous grouting material poured into the void structure of the porous asphalt mixture forms PELAM. The grouting material was thermosetting, and the asphalt binder was a viscoelastic material. With the increase of temperature, the asphalt mixture changes from elasticity to viscosity, resulting in poor adhesion between the asphalt binder and the aggregate, and the PELAM. The ability of the mixture to resist deformation decreased, so the dynamic modulus of the mixture showed a decline trend.

Under the same test temperature, the dynamic modulus of each specimen increased gradually with the increase of loading frequency. Within the range of 0.1–5 Hz, the growth trend of the dynamic modulus of the mixture was relatively fast, while in the 5–25 Hz range, the growth trend slowed down. Under the same loading frequency and test temperature, the larger the void ratio, the greater the dynamic modulus of the mixture. There was a lag between the mechanical response of the asphalt mixture and the periodic load. With the increase of loading frequency, the lag phenomenon shows a weakening trend; part of the energy applied to the specimen cannot be released in time, and the accumulation of energy gradually increases with the increase of loading frequency, increasing dynamic modulus. In addition, the larger the void ratio, the more self-luminous grouting material poured into the porous asphalt mixture, and the dynamic modulus of the cured grouting material was much greater than that of the asphalt mixture. Therefore, as the porosity increases, the dynamic modulus of the PELAM increases.

3.1.2 Phase angle

The phase angle of PELAM with void ratios of 22%, 24%, and 26%, under different temperatures and loading frequencies, was shown in Figure 4. As can be seen, there were obvious differences in the phase angle of specimens at different test temperatures. When the temperature was 5 °C, its phase angle first decreased and then increased and then decreased with the increase of loading frequency. Within the range of 0.1–1 Hz, the phase angle gradually decreased with the increase of loading frequency, while in the 1–5 Hz range, the phase angle showed an increasing trend, and in the 10–25 Hz frequency range, the phase angle decreased with the increase of loading frequency. When the temperature was 20 °C, its phase angle showed a decreasing trend with the increase of loading frequency. When the temperature was 35 °C, the phase angle of specimens with different void ratios all increased with the increase of loading frequency. In the 0.1–1 Hz frequency range, the phase angle increased significantly, while in the 1–25 Hz frequency range, the increase of phase angle was slow.

The change in phase angle reflects the influence of asphalt binder on the structural strength of self luminous asphalt mixture. At 5°C, the phase angle first increases to the peak with the increase of loading frequency, then gradually becomes flat, and then decreases, indicating that at lower temperatures, the PELAM is positively affected by the asphalt binder and its viscosity is strengthened; As the temperature increases, the structure of asphalt mixture becomes unstable, and the interaction between different particle sizes of mineral materials strengthens the overall structural strength of the mixture, resulting in a decrease in phase angle (Xing et al., 2024).

3.1.3 Repeated loading creep

The flow number and microstrain of PELAM with void ratios of 22%, 24%, and 26% are shown in Figure 5. As can be seen, with the increase of void ratio, the flow number gradually increased. The epoxy resin self-luminous grouting material after curing improved the ability of the mixture to resist irreversible deformation and

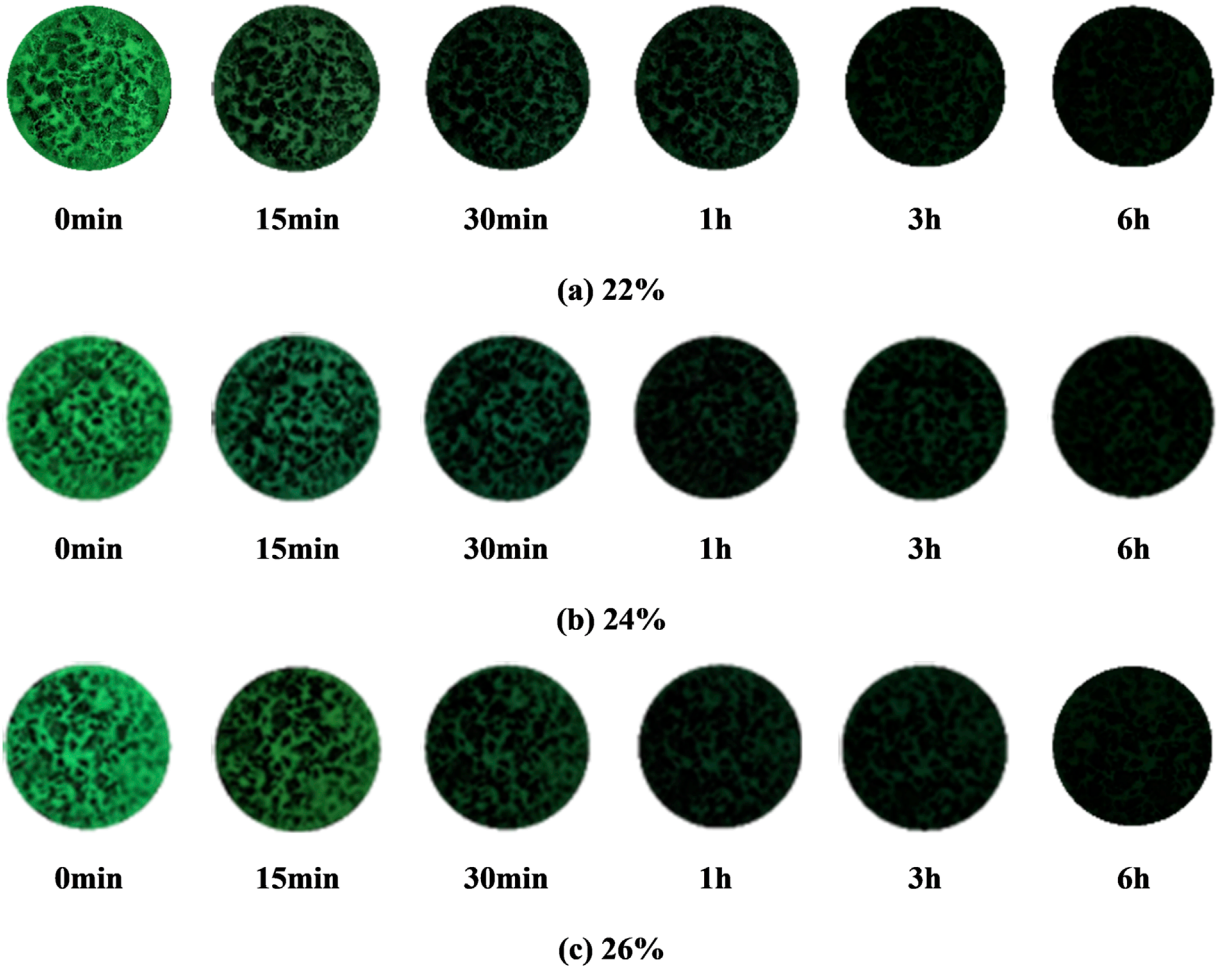

FIGURE 6
Afterglow effect of PELAM specimens with different void ratios.

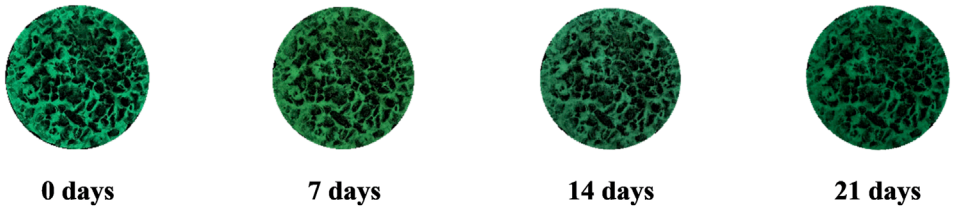

FIGURE 7
Afterglow effect of PELAM specimens under different immersion times.

structural instability at high temperatures, and also made the complex shear modulus of the mixture larger, the cumulative deformation formed by repeated loading decreases, the number of loadings during the compaction period and stable period increased, the material was less likely to enter the plastic failure state, and the high-temperature resistance to permanent deformation was enhanced.

3.2 Analysis of factors affecting luminescent function

3.2.1 Porosity

The afterglow performance of three types of PELAM specimens, each with different void ratios (22%, 24%, and 26%), was tested. As shown in Figure 6, it can be observed that for specimens with

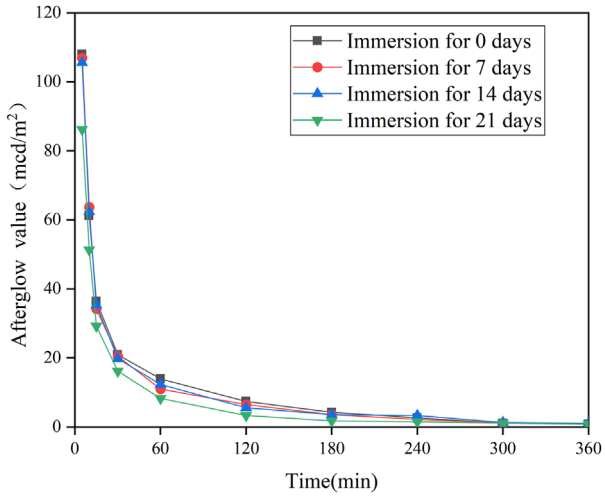

FIGURE 8
Afterglow value of PELAM specimens under different immersion times.

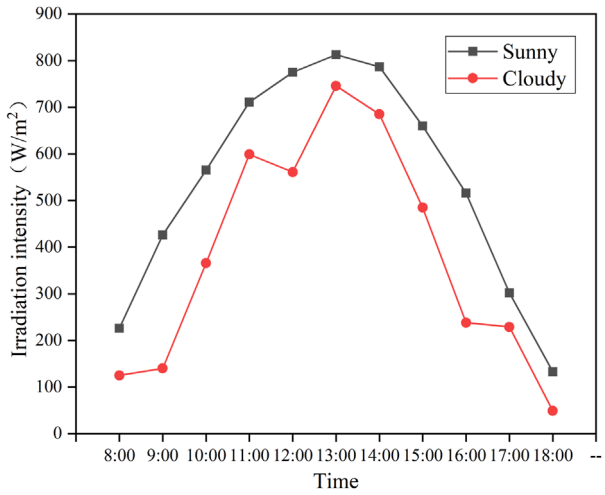

FIGURE 9
Irradiance at different times on sunny and cloudy weather.

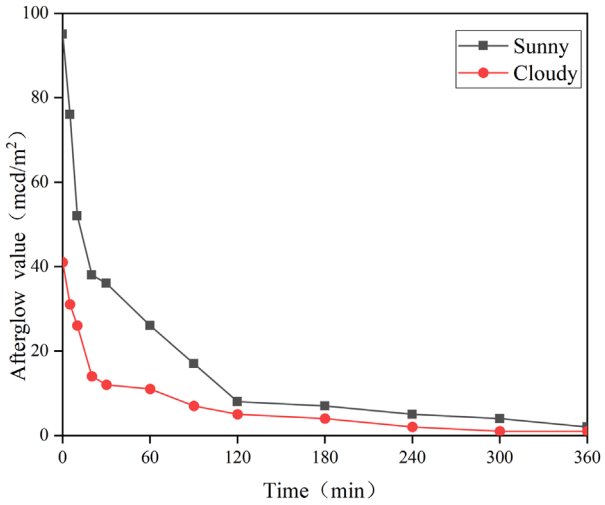

FIGURE 10
Afterglow value of PELAM specimens under sunny and cloudy weather.

the same void ratio, their surface afterglow brightness gradually decreases over time. At the initial stage, the afterglow of all specimens attains its peak brightness, which is then followed by a progressive dimming. Even after 6 h, with a marked reduction in afterglow intensity, the light radiating from the specimens' surfaces remains visible to the naked eye, maintaining a level of luminosity.

At the 15-min mark, the tested samples with different void ratios showed negligible differences in their afterglow luminosity. Specifically, regardless of whether the specimens had a void ratio of 22%, 24%, or 26%, their surface brightness exhibited a good and bright effect, but the brightness were indistinguishable to the human eye. Instrument measurements revealed brightness values of 36 mcd/m^2, 38 mcd/m^2, and 34 mcd/m^2, respectively, suggesting that porosity has minimal impact on the luminescent properties of PELAM. The test focused on the afterglow brightness values on the specimen surfaces for comparison. The PAC-10 mixture, through gradation design, forms distinct porosity structures. However, during specimen preparation, the long-afterglow grout filled the void structure and excess grout was removed to create a specific construction depth. This thin layer of slurry nearly fully covered the specimen surface, resulting in insignificant differences in afterglow brightness among the specimens.

3.2.2 Immersion time

This study tested the afterglow performance of PELAM following immersion durations of 0, 7, 14, and 21 days. Figure 7 displays the afterglow effect of specimens with 26% void ratio at various immersion periods. There was no significant change in the brightness on the surface of the specimens across different immersion times. The afterglow values were recorded as 105.58 mcd/m^2 after 14 days of water immersion and 86.21 mcd/m^2 after 21 days of immersion, representing an approximate 20% decrease in luminance.

To quantitatively represent the afterglow brightness, Figure 8 shows the afterglow value of PELAM specimens under different immersion times within 6 h after excitation. As can be seen that the variation pattern of the afterglow curve under different immersion times was roughly the same. As immersion time progresses, there is a slight decrement in the afterglow brightness of the specimen surface. The long afterglow material is encapsulated within a cured epoxy resin adhesive system, which functions as a water barrier. Initially, the afterglow brightness of the PELAM specimen surface remains largely unchanged. However, once the immersion duration reaches 21 days, water pressure and capillary action allow a fraction of water to slowly penetrate into the long afterglow material, initiating hydrolysis. This process leads to a minor decrease in the afterglow brightness of the specimen.

3.2.3 Weather condition

This study selected sunny and cloudy weather for testing, and collected the irradiance values from 8:00 to 18:00,

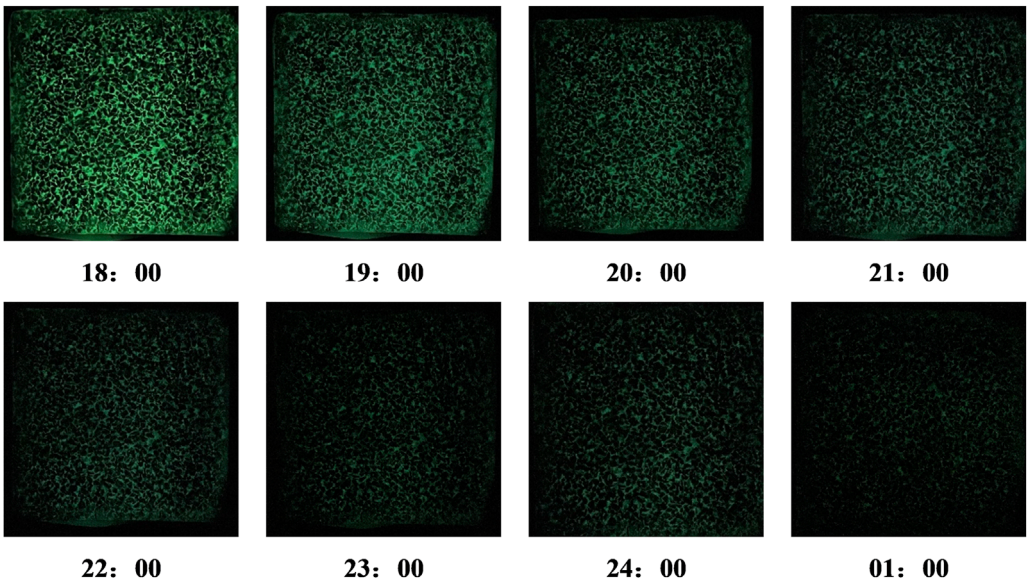

FIGURE 11
Afterglow effect of PELAM specimens in 6 hours under cloudy weather conditions.

as shown in Figure 9. It can be seen that the solar irradiance under sunny weather was always greater than cloudy weather. Before 13:00, the solar irradiance gradually increased; at 13:00, the solar irradiance reached the maximum, the maximum irradiance value on a sunny day is 813 W/m^2, and on a cloudy day, it is 746 W/m^2; after 13:00, the solar irradiance gradually decreased. After 18:00, the solar irradiance was significantly reduced, and the excitation effect on the PELAM specimens was weakened. At 18:00, the specimens were placed in a dark environment, and the changing trend of afterglow brightness with time was tested. Sampling will be conducted every hour starting from 18:00 until 1:00 a.m. the next day.

The test results of afterglow values of PELAM specimens under sunny and cloudy weather are shown in Figure 10. It can be seen from the figure that the afterglow value of PELAM specimens under sunny and cloudy weather showed the same trend, and the afterglow brightness gradually decreased with the extension of time. The afterglow brightness of the specimens under sunny days was significantly higher than that under cloudy days, which was mainly because the long afterglow material was effectively excited under natural light, and the excitation effect under sunny days was better than that under cloudy days. In addition, from the afterglow decay curve, although under cloudy weather conditions, the PELAM specimens still have an obvious luminescent effect after 6 h, with a afterglow value of 1.22 mcd/m^2, exceeding the lowest visible afterglow value of 0.32 mcd/m^2.

The afterglow effect under cloudy weather conditions is shown in Figure 11. It can be seen although under cloudy weather conditions, the PELAM specimens still have an obvious luminescent effect after 6 h, and the human eye can easily identify the luminescent effect of the specimen, indicating that this pouring self-luminous asphalt mixture has good afterglow performance under the excitation of natural light.

4 Conclusion

In this study, the PELAM was formulated. The mixture's mechanical characteristics and luminescent capabilities were examined and assessed. The key findings are summarized as follows.

1. The dynamic modulus of PELAM gradually decreases with the increase of test temperature, and gradually increases with the increase of loading frequency and porosity. Under the same temperature and loading conditions, the PELAM specimen with a 26% void ratio exhibits the highest dynamic modulus.
2. The phase angle of self luminous asphalt mixture poured varies greatly at different temperatures and frequencies, and there is no obvirous regularity in the numerical values.
3. With the increase of porosity, the flow number and the micro-strain corresponding to the flow number of PELAM increase gradually, and the resistance to permanent deformation at high temperatures is enhanced.
4. Porosity and short-term immersion have little effect on the afterglow effect of PELAM. The afterglow brightness is slightly reduced after 21 days of immersion; under the excitation of natural light, the afterglow brightness of PELAM within the range recognizable by the human eye can last for more than 6 h.

Data availability statement

The original contributions presented in the study are included in the article, further inquiries can be directed to the corresponding author.

Author contributions

WJ: Funding acquisition, Project administration, Writing – review and editing. SS: Data curation, Methodology, Validation, Writing – review and editing. PL: Writing – original draft, Writing – review and editing. JS: Investigation, Writing – review and editing. CX: Formal Analysis, Writing – review and editing.

Funding

The author(s) declare that financial support was received for the research and/or publication of this article. This project was jointly supported by the Key-Area Research and Development Program of Guangdong Province (Grant No. 2019B111105002).

Conflict of interest

Author WJ was employed by Shenzhen-Zhongshan Link Administration Center.

Author SS was employed by Guangdong Highway Construction Co., Ltd.

The remaining authors declare that the research was conducted in the absence of any commercial or financial relationships that could be construed as a potential conflict of interest.

Generative AI statement

The author(s) declare that no Generative AI was used in the creation of this manuscript.

Any alternative text (alt text) provided alongside figures in this article has been generated by Frontiers with the support of artificial intelligence and reasonable efforts have been made to ensure accuracy, including review by the authors wherever possible. If you identify any issues, please contact us.

Publisher's note

References

Al-shawafi, A., Zhu, H., Haruna, S. I., Bo, Z., Laqsum, S. A., and Borito, S. M. (2023). Impact resistance of ultra-high-performance concrete retrofitted with polyurethane grout material: experimental investigation and statistical analysis. *Structures* 55, 185–200. doi:10.1016/j.istruc.2023.06.043

Cai, J., Pei, J., Luo, Q., Zhang, J., Li, R., and Chen, X. (2017). Comprehensive service properties evaluation of composite grouting materials with high-performance cement paste for semi-flexible pavement. *Constr. Build. Mater.* 153, 544–556. doi:10.1016/j.conbuildmat.2017.07.122

Caputo, P., Porto, M., Angelico, R., Loise, V., Calandra, P., and Oliviero Rossi, C. (2020). Bitumen and asphalt concrete modified by nanometer-sized particles: basic concepts, the state of the art and future perspectives of the nanoscale approach. *Adv. Colloid Interface Sci.* 285 (275), 102283. doi:10.1016/j.cis.2020.102283

Cavalli, M. C., Chen, D., Chen, Q., Chen, Y., Cannone Falchetto, A., Fang, M., et al. (2023). Review of advanced road materials, structures, equipment, and detection technologies. *J. Road Eng.* 3 (4), 370–468. doi:10.1016/j.jreng.2023.12.001

Chen, Z., Qiao, J., Yang, X., Sun, Y., and Sun, D. (2023). A review of grouting materials for pouring semi-flexible pavement: materials, design and performance. *Constr. Build. Mater.* 379, 131235. doi:10.1016/j.conbuildmat.2023.131235

Dalhat, M. A., and Al-Adham, K. (2023). Review on laboratory preparation processes of polymer modified asphalt binder. *J. Traffic Transp. Eng. Engl. Ed.* 10 (2), 159–184. doi:10.1016/j.jtte.2023.01.002

Hamid, A. M., Abbas, I. S., and Canakci, H. (2023). Influence of mechanochemical activation on the rheological, fresh and mechanical properties of one-part geopolymer grout. *Adv. Cem. Res.* 35 (3), 96–110. doi:10.1680/jadcr.21.00205

He, L., Huang, H., and den Wim, V. (2020). A state-of-the-art on microcapsules for asphalt self-healing. *Mater. Rep.* 34 (15), 15092–15101. doi:10.11896/cldb.19060096

Jia, M., Sha, A., Jiang, W., Li, X., and Jiao, W. (2023). Developing a solid–solid phase change heat storage asphalt pavement material and its application as functional filler for cooling asphalt pavement. *Energy Build.* 285, 112935. doi:10.1016/j.enbuild.2023.112935

Jiang, W., Wang, T., Yuan, D., Sha, A., Zhang, S., Zhang, Y., et al. (2023a). Available solar resources and photovoltaic system planning strategy for highway. *Renew. Sustain. Energy Rev.* 203, 114765. doi:10.1016/j.rser.2024.114765

Jiang, W., Li, P., Xing, C., Xiao, J., Wang, P., and Bai, L. (2023b). Development and performance of pouring self-luminescent asphalt mixture. *J. Clean. Prod.* 414, 137637–137637.14. doi:10.1016/j.jclepro.2023.137637

Khan, M. I., Sutanto, M. H., Napiah, M. B., Zoorob, S. E., Al-Sabaeei, A. M., Rafiq, W., et al. (2021). Investigating the mechanical properties and fuel spillage resistance of semi-flexible pavement surfacing containing irradiated waste PET based grouts. *Constr. Build. Mater.* 304, 124641. doi:10.1016/j.conbuildmat.2021.124641

Li, X., Hao, M., Zhong, Y., Zhang, B., Wang, F., and Wang, L. (2020). Experimental study on the diffusion characteristics of polyurethane grout in a fracture. *Constr. Build. Mater.* 273, 121711. doi:10.1016/j.conbuildmat.2020.121711

Li, P., Yang, T., Ma, P., Fei, X., Li, F., Ye, J., et al. (2022). Luminous and bonding performance of self-luminescent cementitious coatings based on white cement and geopolymer. *Constr. Build. Mater.* 362, 129814. doi:10.1016/j.conbuildmat.2022.129814

Li, C., Chen, F., Lin, Z., Jiang, M., and Lin, H. (2024). Application efect of selfluminous road markings at entrance of crossriver and crosssea tunnel. *J. Chang'an Univ. Nat. Sci. Ed.* 44 (02), 101–114. doi:10.19721/j.cnki.1671-8879.2024.02.010

Li, H., Xing, C., Zhu, B., Zhang, X., Gao, Y., Tang, S., et al. (2025). Comparative analysis of four styrene-butadiene-styrene (SBS) structure repair agents in the rejuvenation of aged SBS-Modified bitumen. *Constr. Build. Mater.* 476, 141232. doi:10.1016/j.conbuildmat.2025.141232

Ling, S., Hu, M., Sun, D., and Xu, L. (2021). Mechanical properties of pouring semi-flexible pavement material and engineering estimation on contribution of each phase. *Constr. Build. Mater.* 315, 125782. doi:10.1016/j.conbuildmat.2021.125782

Ling, S., Itoua, P. I., Sun, D., and Jelagin, D. (2022). Damage characterization of pouring semi-flexible pavement material under triaxial compressive load based on X-ray computed tomography. *Constr. Build. Mater.* 348, 128653. doi:10.1016/j.conbuildmat.2022.128653

Liu, W., Zhang, S., and Li, Y. (2023). The expansion and mechanical property-based cavity expansion model for polyurethane grouting underneath the airport pavement. *Transp. Geotech.* 43, 101141. doi:10.1016/j.trgeo.2023.101141

Mishra, B., and Gupta, M. K. (2018). Use of randomly oriented polyethylene terephthalate (PET) fiber in combination with fly ash in subgrade of flexible pavement. *Constr. Build. Mater.* 190, 95–107. doi:10.1016/j.conbuildmat.2018.09.074

Saleh, S., Yunus, N. Z. M., Ahmad, K., and Ali, N. (2019). Improving the strength of weak soil using polyurethane grouts: a review. *Constr. Build. Mater.* 202, 738–752. doi:10.1016/j.conbuildmat.2019.01.048

Shan, J., Jiang, W., Huang, Y., Yuan, D., and Liu, Y. (2024). Unmanned aerial vehicle (UAV)-based pavement image stitching without occlusion, crack semantic segmentation, and quantification. *IEEE Trans. Intelligent Transp. Syst.* 25 (11), 17038–17053. doi:10.1109/TITS.2024.3424525

Sharkawi, A., Taman, M., Afefy, H. M., and Hegazy, Y. (2020). Efficiency of geopolymer vs. high-strength grout as repairing material for reinforced cementitious elements. *Structures* 27, 330–342. doi:10.1016/j.istruc.2020.06.001

Wang, C., Li, Z., and Zhou, Z. (2022a). Compatibility of different fibres with red mud-based geopolymer grouts. *Constr. Build. Mater.* 315, 125742. doi:10.1016/j.conbuildmat.2021.125742

Wang, W., Sha, A., Falchetto, A. C., Wang, D., Jiang, W., and Li, X. (2022b). Properties analysis of self-luminous cement-based materials with different colors and their visual comfort evaluation on pavement. *Sol. Energy* 247, 214–227. doi:10.1016/j.solener.2022.10.013

Wang, J., Hong, J., and Zhang, Y. (2023a). Interfacial adhesion mechanism of cement grout asphalt composite material. *J. Chin. Ceram. Soc.* 51 (07), 1660–1669. doi:10.14062/j.issn.0454-5648.20220838

Wang, W., Jiao, W., Sha, A., Li, X., Jiang, W., and Yuan, D. (2023b). Study on the mechanics and functionalities of self-luminous cement-based materials with energy storage and slow release properties. *Sol. Energy* 259, 72–85. doi:10.1016/j.solener.2023.04.049

Xing, C., Tang, S., Chang, Z., Hang, Z., Li, H., and Zhu, B. (2024). A comprehensive review on the plant-mixed cold recycling technology of emulsified asphalt: raw materials and factors affecting performances. *Constr. Build. Mater.* 439, 137344. doi:10.1016/j.conbuildmat.2024.137344

Xiong, K., Zhang, J., He, Y., Li, J., Zhang, M., Li, R., et al. (2024). Introducing the mineral powder to strengthen polyurethane grouting materials for crack repair of asphalt pavements. *Constr. Build. Mater.* 453, 139023. doi:10.1016/j.conbuildmat.2024.139023

Zhang, Y., Wang, Y., Wu, Z. G., Lu, Y. M., Kang, A. H., and Xiao, P. (2021). Optimal design of geopolymer grouting material for semi-flexible pavement based on response surface methodology. *Constr. Build. Mater.* 306, 124779. doi:10.1016/j.conbuildmat.2021.124779

Zhang, D., Bu, W., Wang, Q., Liu, P., Shao, Z., Liu, X., et al. (2023). A review of recent developments and challenges of using phase change materials for thermoregulation in asphalt pavements. *Constr. Build. Mater.* 400, 132669. doi:10.1016/j.conbuildmat.2023.132669

Zheng, X. G., Wu, L., and Shui, L. (2023). Road performance of high performance pouring semi-flexible pavement material. *J. of Build. Mat.* 26 (6), 638–643+652. doi:10.1016/j.conbuildmat.2023.131235